Monte Carlo Simulation of Neoclassical Transport in Axisymmetric and Ripple Tokamaks

W. Lotz and J. Nührenberg
Max-Planck-Institut für Plasmaphysik, EURATOM-Association, Garching

Z. Naturforsch. **37a**, 899–905 (1982); received May 13, 1982

To Professor Arnulf Schlüter on his 60th Birthday

Simple axisymmetric and ripple tokamak model fields are used to compute neoclassical transport coefficients by Monte Carlo simulation over a wide range of mean free paths in the approximation of small gyroradius. Further assumptions are a monoenergetic particle distribution which is only subject to pitch angle scattering and a vanishing electric field. Pfirsch-Schlüter, plateau, banana and ripple transport coefficients are obtained. In the ripple regime the description is unified by introducing the concept of an effective ripple. Cases in which ripple transport is diminished due to collisionless detrapping are observed.

I. Introduction

The development of Monte Carlo codes for the simulation of neoclassical transport [see, for example, 1–3] has been carried out following mainly two approaches. Apart from their use for model problems, the elegant magnetic coordinates [2] have to be supplemented by a code computing the strength of the magnetic field $\boldsymbol{B}$ [4]; they have the advantage of an easy way to incorporate an electric field and the disadvantage of being less applicable to magnetic configurations with islands or ergodic field lines. On the other hand, codes using given magnetic fields [1, 3] are straightforward, self-consistent in the sense that no hypothetical structure of $|\boldsymbol{B}|$ occurs [5], and are easily adaptable to various physical situations; an electric field cannot so easily be incorporated and, possibly, they are not as efficient computationally, although a detailed comparison remains to be done.

The Monte Carlo code used here was mainly developed to study neoclassical transport in stellarators and preliminary results have been reported [3, 6]. In Sect. II a brief outline of the code is given; Sect. III describes the model fields for the axisymmetric and the ripple tokamak; Sect. IV reports results for the axisymmetric, Sect. V for the ripple tokamak as a simple example of asymmetric configurations whose $1/\nu$ transport behaviour in the long mean free path regime has been controversial (see, e.g. [1, 7, 8]); Sect. VI discusses the dependence of the results on various numerical and physical parameters; conclusions are presented in Section VII.

Reprint requests to Max-Planck-Institut für Plasmaphysik, Bibliothek, D-8046 Garching.

II. Outline of the Monte Carlo Code

Here, the way is described in which the magnetic field, the particle trajectories and the Monte Carlo simulation of collisions are implemented into the code.

Magnetic fields are represented by their Cartesian components in a Cartesian coordinate system. If the field is given in analytical form its three components and their eight (because of $\nabla \cdot \boldsymbol{B} = 0$) independent derivatives are used. If the field is obtained from line currents via Biot-Savart's law the three field components and the five (because of $\nabla \cdot \boldsymbol{B} = \nabla \times \boldsymbol{B} = 0$) independent derivatives are used. For sufficiently complicated analytical fields [9] and, in any case, for fields obtained from coils, the field components and their derivatives are stored in a 3D grid, usually in a $20 \times 17 \times 17$ grid per field period, and interpolated as needed. This way of handling the magnetic field is particularly useful to reduce the computing time on the CRAY-1, for which this code was implemented (see also below).

Particle trajectories are treated in the guiding center approximation with the usual guiding center equations

$$\boldsymbol{v} = v_\parallel \boldsymbol{B}/B + \frac{m}{e B^2} \boldsymbol{B} \times (v_\parallel^2 \boldsymbol{\varkappa} + \tfrac{1}{2} v_\perp^2 \nabla B/B),$$

$$\dot{v}_\parallel = -\frac{1}{2} \frac{v_\perp^2}{B^2} \boldsymbol{B} \cdot \nabla B, \qquad (1)$$

0340-4811 / 82 / 0800-0899 $ 01.30/0. — Please order a reprint rather than making your own copy.

where $B = |\boldsymbol{B}|$; $\boldsymbol{\varkappa}$ is the field line curvature and

$$\boldsymbol{B} \times \boldsymbol{\varkappa} = \frac{1}{B} \boldsymbol{B} \times \nabla B + \nabla \times \boldsymbol{B} - \boldsymbol{B} \cdot (\nabla \times \boldsymbol{B}) \boldsymbol{B} / B .$$

More recent formulations [10] have not yet been taken into account.

These equations (in Cartesian coordinates) are numerically integrated with the method of Runge-Kutta-Gill ([11], see Table 1) which is of fourth order and contains a correction for the rounding error. For each time step the field components and their derivatives are needed five times. The Runge-Kutta step size is held constant during one run (see below) and is chosen as large as possible for the configuration under consideration; in the case of many field periods the time step τ corresponds to a motion which covers only a small fraction of a period.

Table 1. Fortran program used to integrate magnetic field lines, particle trajectories or guiding center trajectories using the method of Runge-Kutta-Gill.

```
C
      SUBROUTINE YDIR (K, H, N, SYSTEM)
C
C
      IMPLICIT REAL*8 (A-H, O-Z)
C
      DIMENSION    A(4), AP(4), C(4)
C
      COMMON /TR/  P(7), F(7), Q(7)
C
      DATA A   /  0.5                  D0,
     1             0.2928932188134524 D0,
     2             1.7071067811865475 D0,
     3             0.1666666666666666 D0/
      DATA C   /-1.                    D0,
     1            -0.2928932188134524 D0,
     2            -1.7071067811865475 D0,
     3            -0.3333333333333333 D0/
C
        AP(1) = A(1)*H
        AP(2) = A(2)*H
        AP(3) = A(3)*H
        AP(4) = A(4)*H
C
      DO 400 L = 1, K
C
      DO 200 J = 1, 3
      CALL SYSTEM
      DO 200 I = 1, N
          R    = Q(I)*C  (J)
          T    = F(I)*AP(J)
          R    = R + T
          P(I) = P(I) +R
  200     Q(I) = Q(I) +3.*R -T
C
      CALL SYSTEM
      DO 300 I = 1, N
          R    = Q(I)*C  (4)
          T    = F(I)*AP(4)
          R    = R +T
          P(I) = P(I) +R
  300     Q(I) = Q)I) +3.*(R -T)
C
  400 CONTINUE
C
      RETURN
C
      END
```

As Monte Carlo equivalent of the pitch angle scattering process [12, 2] Boozer's representation [2]

$$\lambda_n = \lambda_0 (1 - \Delta) \pm \sqrt{(1 - \lambda_0^2) \Delta} \tag{2}$$

is used where $\lambda = v_\parallel / v$ and λ_n and λ_0 are the new and the old value of this quantity; $v_\perp$ is changed accordingly so that the particle energy is constant. The quantity $\Delta (\ll 1)$ represents the small angle collisions ($v_\parallel / v = \cos\theta$, $\Delta\theta \approx \sqrt{\Delta}$); the $\pm$ sings are taken randomly. The collision time corresponding to 90° collisions is defined as $\tau_{90°} = \tau / \Delta$ ($\nu_c = \Delta / \tau$); the mean free path as $\Lambda = \tau_{90°} v = \tau v / \Delta$.

The choice of the free parameters Δ and particle energy E for the evaluation of ion transport in the limit of small gyroradius is obtained as follows. For a given Λ, the ratio of gyroradius to plasma radius is chosen so small (in practice simply by choosing the particle energy) that

$$v_D \tau_{90°} / r_0 \ll 1 , \tag{3}$$

where v_D characterizes a typical drift velocity perpendicular to the field and r_0 the mean radius of the magnetic surface considered. In simple tokamak or stellarator cases

$$v_D \sim E / e B R$$

as is obvious from (1), so that

$$\frac{\Lambda_{\text{eff}}}{R} \cdot \frac{\varrho}{r_0} \ll 1 \tag{4}$$

is the dimensionless quantity which is chosen small (R toroidal radius, ϱ gyroradius). Here, Λ_{eff} is the effective mean free path over which the above drift occurs, e.g. $\Lambda_{\text{eff}} \approx \delta \Lambda$ for a tokamak with ripple δ. The inequality (3) entails $\tau_{90°}$, which in turn determines Δ in such a way that $\Delta \to 0$, for increasing Λ if the collision operator (2) is applied after every time step τ.

Once ϱ / r_0 and Δ are chosen, a random sample of particles (usually 64 or 100) is started on a magnetic surface whose transport coefficient is to be

determined, distributed randomly within a period in this surface and with respect to λ. The particles are advanced "simultaneously" according to (1) and (2), in order to exploit the vector mode of the CRAY-1. Their deviations from the magnetic surface are monitored; the run is continued until their mean square deviation divided by time becomes constant apart from the statistical error.

III. Model Fields

For the simulation of the axisymmetric tokamak, a simple divergencefree field [13] is used

$$B_\varphi = B_0 \frac{R_0}{R}\,,\; B_\theta = B_0 \iota_0 \frac{r}{R}\,, \tag{5}$$

where φ is the toroidal angle, θ the poloidal angle measured around the radius of the magnetic axis R_0, R is the major radius, r the minor radius of the circular surfaces, ι_0 the rotationa transform on the magnetic axis.

For the simulation of ripple tokamaks the field generated by circular line currents lying in planes $\varphi = \text{const}$ with centers in the equatorial plane was superimposed on the field given by (5). For purposes of comparison [7], 36 such loops, every second one of which carries the same amount but antiparallel current, were used to represent 18 toroidal field coils.

Varying the amount of current and the position of the loops allows to vary the ripple depth and its spatial distribution.

IV. Results for the Axisymmetric Tokamak

First, the classical result [14] for the tokamak

$$D_B \sim A^{3/2} D_P/\Lambda\,,\quad D_P \sim \varrho^2 v/\iota R_0\,,$$
$$D_{PS} \sim D_P/\Lambda\,,$$

is reproduced as a test for the code. Here v and ϱ are velocity $[v = (2E/m)^{1/2}]$ and formal gyroradius associated with v, $\varrho = mv/eB_0$. The plateau value which can be defined with good accucary for $A \geqq 20$ (see Fig. 1) is found to be

$$D_P = (1.27 \pm 0.02)\,\varrho^2 \frac{v}{\pi \iota R_0} \tag{6}$$

and 0.02 is the statistical error.

Equation (6) is used as a reference value to define a dimensionless transport coefficient D^* by

$$D^* = D/D_P\,,\quad D_P^* = 1\,. \tag{7}$$

Further, a dimensionless mean free path is introduced by

$$L^* = \Lambda/L_c\,,$$

where the reference length L_c is half the connection length

$$L_c = \pi R_0/\iota\,.$$

Thus, (6) may be interpreted as obtained by random walk with step size ϱ/ι and collision frequency v/L_c.

In the banana regime the transport coefficient is found to be (see Fig. 1)

$$D_B^* \approx A^{3/2}/L^*, \tag{8}$$

where it must be noted that in the regime covered numerically the proportionality to L^{*-1} is only approximately valid.

Finally, in the Pfirsch-Schlüter regime, the transport coefficient turns out to be (see Fig. 1)

$$D^* = 1/L^* \tag{9}$$

which motivated the choice of the reference length L_c.

For the results shown in Fig. 1 the rotational transform varied between 0.5 and 2.0, so that the ι-dependence of (7)—(9) is verified as well. Equation (9) does not completely reproduce the Pfirsch-Schlüter enhancement factor [13]

$$1 + 2/\iota^2$$

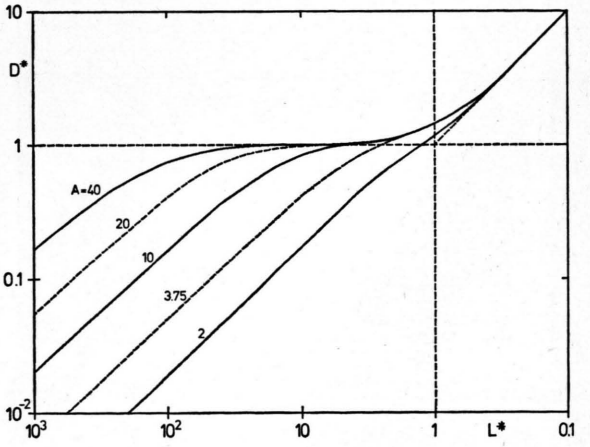

Fig. 1. Normalized diffusion coefficient $D^* = D/D_p$ versus normalized mean free path $L^* = \Lambda/L_c$ (corresponding to collisionality $1/L^*$) for tokamaks of various aspect ratios A and rotational transforms ($0.5 \leqq \iota \leqq 2$). D_p is the transport coefficient of the plateau regime, L_c is half the connection length.

since the collision operator only changes the pitch angle and not the location of the guiding center. Thus, the classical diffusion of guiding centers is not contained.

The approximation (4) is discussed in Section VI.

V. Results for the Tokamak with Ripple

First, the standard situation treated in the theoretical literature is analyzed, in which the toroidal field has a ripple of the form

$$B_T \approx B_0\left(1 - \frac{1}{A}\cos\theta - \delta_0 \cos N\varphi\right). \quad (10)$$

This situation is obtained if the current loops generating the ripple enclose the plasma and are suitably positioned.

Numerical results were obtained for $A = 3.75$, $N = 18$, various ripples δ_0, and values of ι, see Figure 2. The parameter $K = NA\,\delta/\iota$ which determines the ripple depth as evaluated along a field line [15] varies from values large compared to unity to values well below unity. In all cases the results verified the classical prediction [16]

$$D_R \sim \delta^{3/2}/\nu\,.$$

Since the deviation of a drifting trapped particle from its magnetic surface is proportional to $\sin\theta$, it is natural to try to find a unified description of the numerical results by defining an effective ripple depth

$$\delta_e^{3/2} = \frac{\int \delta^{3/2}(\theta)\sin\theta\,d\theta}{\int \sin\theta\,d\theta}\,,$$

where $\delta(\theta)$ is obtained by evaluation of the ripple along a field line. Indeed, the results can be summarized by

$$D_R^* = (1.65 \pm 0.10)\,\delta_e^{3/2} L^* \quad (11)$$

as shown in Figure 2. Thus, ripple transport is comparable to plateau transport for

$$\delta_e^{3/2} L^* \sim 1\,.$$

Comparison with the small gyroradius approximation (4) leads to the limitation

$$\frac{\varrho}{r_0} \ll \frac{\iota}{\pi}\,\delta_e^{1/2}\,.$$

Thus, for realistic parameters, ripple transport as discussed here will not be valid for values which are much larger than the plateau value.

On the other hand, these results do not suggest that the range of validity of (11) is restricted to values of D_R^* much smaller than unity as found in [7]. The particular case treated there corresponds to the lowest curve of Fig. 2, which could not be followed to larger values of L^* due to prohibitively large computing time.

Second, a situation is analyzed in which it is computationally easier than with the ripple law (10) to study collisionless detrapping. The current loops

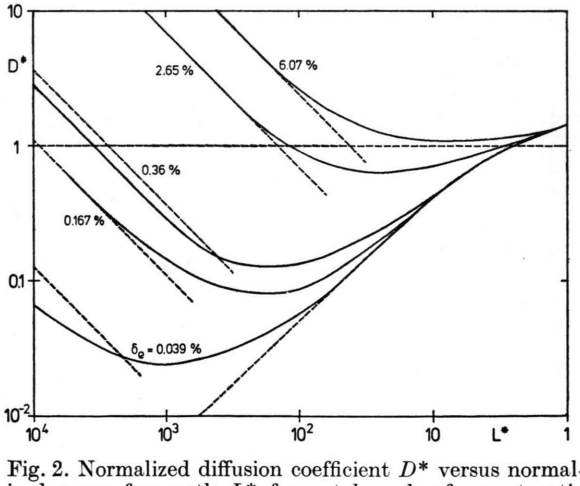

Fig. 2. Normalized diffusion coefficient D^* versus normalized mean free path L^* for a tokamak of aspect ratio $A = 3.75$, rotational transform $\iota = 0.33$ or $\iota = 0.96$, with ripple (number of periods $N = 18$) of various effective ripple depths δ_e. Dashed lines represent the equation $D^* = 1.65\,\delta_e^{3/2} L^*$, while the dashed line at the bottom represents the tokamak without ripple. The ripple field varies only weakly poloidally and is approximately as large on the inner side as on the outer side (see (10)).

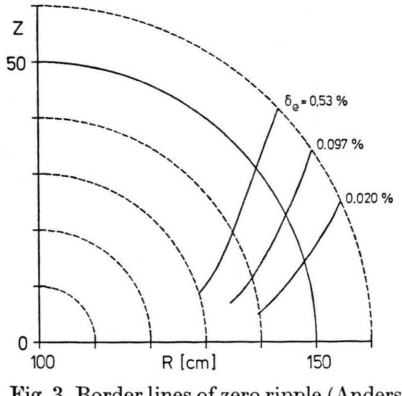

Fig. 3. Border lines of zero ripple (Anderson-Furth-diagram) for the three cases of Figure 4. The minor radius of the magnetic surface used is $r_0 = 50$ cm, the major radius $R_0 = 100$ cm, the aspect ratio $A = R_0/r_0 = 2$. The ripple is produced by current loops of radius 10 cm with centers at $R = 190$ cm, $z = 0$ cm.

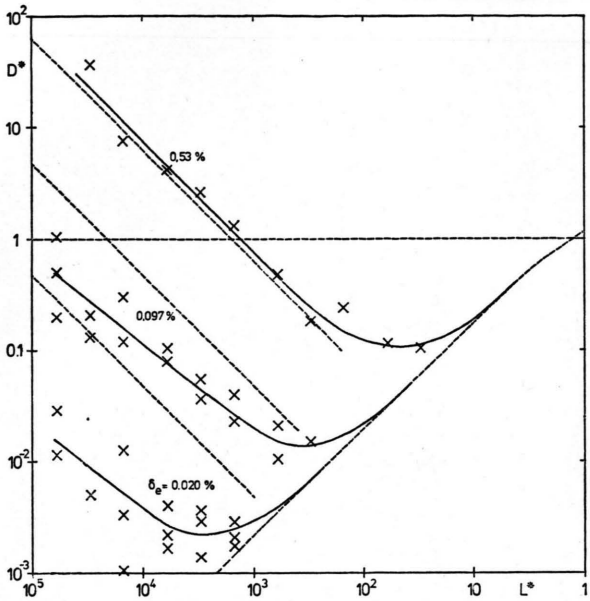

Fig. 4. Normalized diffusion coefficient D^* versus normalized mean free path L^* for a tokamak of aspect ratio $A=2$, rotational transform $\iota=0.96$ with ripple ($N=18$) of various effective ripple depths δ_e. Dashed lines represent $D^*=1.65\,\delta_e^{3/2}\,L^*$, while the dashed line at the bottom represents the tokamak without ripple. The ripple field is concentrated on the outer side of the torus as shown in Fig. 3; there is no ripple on the inner side. Crosses mark results (various gyroradii, $10^{-4}\leqq\varrho/r_0\leqq10^{-2}$) while solid lines are drawn for best fit.

generating the ripple do not enclose the plasma but are placed radially outside. This leads to a concentration of the ripple on the outer side of the plasma with larger peak values of the ripple than obtained with (10) for the same δ_e. Figure 3 shows the Anderson-Furth [15] diagrams, Fig. 4 the numerical results together with the predictions according to (11). While the results are clearly compatible with collisionless detrapping being important for the lower two values of ripple, the possible saturation of D^* with increasing L^* was again outside the computing possibility.

VI. Dependence of Results on Numerical Parameters

Here, the dependence of the results on the small angle parameter Δ [see (2)], the number of collision times, and the ratio of the gyroradius to the radius of the magnetic surface considered are discussed.

1. According to the description of Sect. II, the change in pitch angle given by Δ [see (2)] is usually applied after each integration step. Thus, for short mean free path ($L^*=0.1$) $\Delta\sim0.5$ while for long mean free path ($L^*>10^2$) $\Delta<10^{-3}$. To test this choice of Δ several cases were computed in which the integration step and the application of the collision operator were decoupled. Figure 5 shows results for small and large values of L^* in cases with and without ripple. Generally, the dependence of D^* on Δ is weak. However, small Δ is indeed appropriate for large L^* in particular for ripple cases. This is of course in accordance with the expectation, that completely collisionless drifts should be avoided while determining the ripple transport-coefficient.

2. As described in Sect. II, the number of collision times N_c is chosen such that the mean square deviation from the magnetic surface divided by time be constant. N_c is a strong function of L^*. At small L^* a large value of N_c is needed as is seen from Figure 6. Apparently this is due to the fact

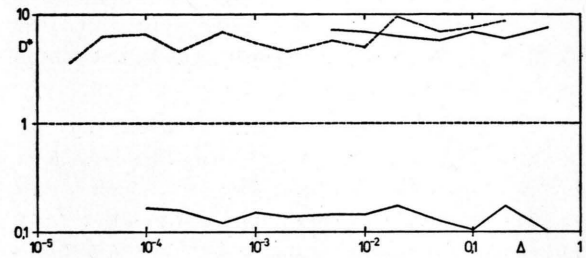

Fig. 5. Computed diffusion coefficient D^* versus small angle parameter Δ (see (2)). Solid curves: tokamak without ripple, $A=3.75$; upper curve: $L^*=0.15$, lower curve: $L^*=30$. Dashed curve: tokamak with ripple $\delta_e=4.55\%$, $A=3.75$, $L^*=300$.

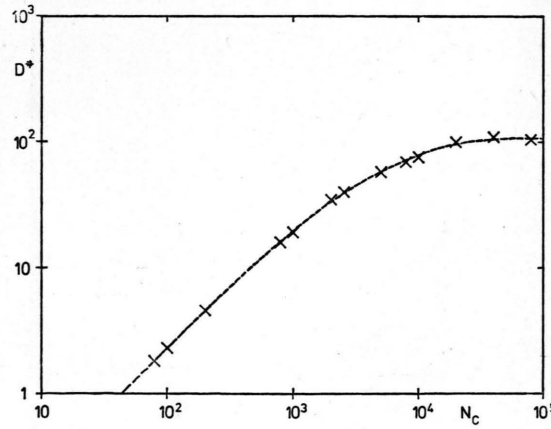

Fig. 6. Computed diffusion coefficient D^* versus number of collision times N_c used. Tokamak without ripple, $A=3.75$, $\iota=0.33$, $L^*=0.01$. Crosses represent computed values, the dashed curve has been drawn for best fit.

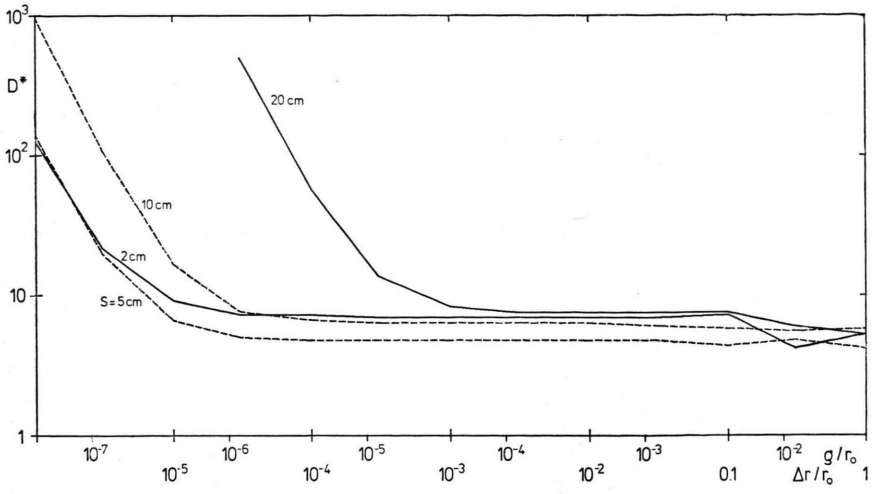

Fig. 7. Computed diffusion coefficient D^* versus ratio of gyroradius ϱ to radius r_0 of the magnetic surface considered or versus mean relative deviation from that magnetic surface for various Runge-Kutta step sizes S. Tokamak without ripple, $A = 3.75$, $R_0 = 100$ cm, $r_0 = 26.7$ cm, $\iota = 0.96$, $B_0 = 2\ T$, deuterons, $L^* = 0.15$.

that sampling the magnetic surface by an individual particle is slowed down by the collisions. For large L^*, generally $N_c \sim 1 - 10$ is sufficient to determine the transport coefficient.

3. To be safely below the limit given by (4), the ratio of gyroradius to the radius of the magnetic surface considered is usually chosen in such a way that the relative root mean square deviation from that surface is of the order of 10^{-2} when D^* has saturated with time. Additional tests (see Figs. 7 and 8) indicate the range of ϱ/r_0 over which the transport coefficient can be computed. For very small ratios ($\varrho/r_0 \sim 10^{-5}$) numerical errors (e.g. the integration error, see Figs. 7 and 8) have to be kept sufficiently small. For $\varrho/r_0 > 10^{-5}$ there is a significant range ($\varrho/r_0 < 10^{-3} \div 10^{-2}$) in which D^* does not depend on ϱ/r_0.

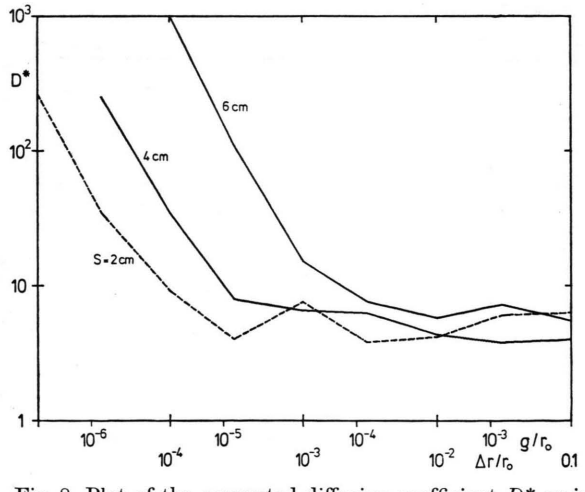

Fig. 8. Plot of the computed diffusion coefficient D^* as in Figure 7. Tokamak with ripple, same parameters as in Fig. 7, except $L^* = 300$ and effective ripple dephth $\delta_e = 4.55\%$.

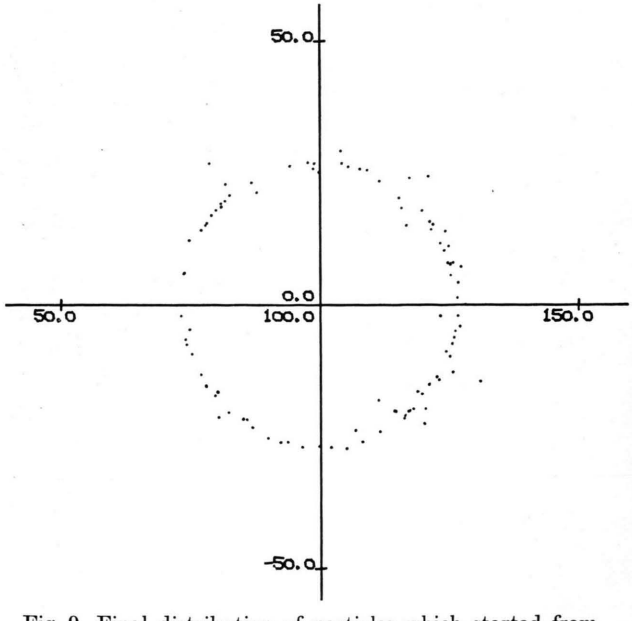

Fig. 9. Final distribution of particles which started from a circular magnetic surface of a tokamak with ripple. Data are $A = 3.75$, $R_0 = 100$ cm, $r_0 = 26.7$ cm, $\iota = 0.96$, $\delta_0 = 6.4\%$ (Eq. (10)), $\delta_e = 4.55\%$, $B_0 = 2\ T$, deuterons, $E = 100$ eV, $\varrho/r_0 = 0.004$, $L^* = 300$, $\Delta r/r_0 = 0.07$, $D^* = 4.3$.

This is the range of applicability of the standard neoclassical theory which starts from a Maxwellian distribution function as zeroth order. The upper bound of this range depends on the physical situation. If the configuration is twodimensional (here tokamak without ripple) rather large values of ϱ/r_0 exceeding 10^{-2} are acceptable and lead to a relative root mean square deviation of order one. For threedimensional configurations with unconfined collisionless particle drifts (here the tokamak with ripple) a loss cone in velocity space appears at large values of L^*, see (4), so that a local transport coefficient can no longer be determined. In the example considered in Fig. 8 ($L^* = 300$, $\delta_e \approx 4.5\%$, $\iota \approx 1$, $D^* \approx 8$) the limit of ϱ/r_0 is approximately $3 \cdot 10^{-3}$, in accordance with the estimate (see Sect. V)

$$\varrho/r_0 \ll \frac{\iota}{\pi} \frac{\delta_e^{1/2}}{D^*} .$$

Figure 9 shows the actual distribution of particles for such a case, which is clearly not dominated by collisionless drift loss.

VII. Summary

A Monte Carlo code for neoclassical transport relying on straightforward evaluation of guiding center orbits in given magnetic fields and Boozer's pitch angle collision operator has been described; energy scattering and electric fields are not yet taken into account. Results for axisymmetric and ripple tokamaks have been reported. Neoclassical theory (PS, plateau, banana, and ripple transport) has been verified. In the ripple regime the description of the results is unified by introducing the concept of an effective ripple δ_e. The upper bound of the range of validity of the standard neoclassical theory (or, equivalently, the appearance of a loss cone in velocity space for large mean free path) has been discussed and indicates that $D^* \sim 1$ may indeed occur for ripples in the percent range and $\varrho/r_0 \sim 10^{-3} - 10^{-2}$. The effect of collisionless detrapping has been observed.

The same code was already applied to stellarator cases [3, 6]; a more complete account of that work is being prepared.

[1] R. E. Potok, P. A. Politzer, and L. M. Lidsky, Proc. of the Sherwood Meeting (1980), 3B23; Phys. Rev. Letters **45**, 1328 (1980).
[2] G. Kuo-Petravic and A. H. Boozer, Proc. of the Sherwood Meeting (1980), 2C9; A. H. Boozer and G. Kuo-Petravic, Phys. Fluids **24**, 851 (1981).
[3] W. Lotz and J. Nührenberg, Proc. of the Sherwood Meeting (1981), 3B41.
[4] A. H. Boozer, Report PPPL-1775, 1981.
[5] H. F. Mynick, T. K. Chu, and A. H. Boozer, Report PPPL-1822, 1981.
[6] R. Chodura, W. Dommaschk, F. Herrnegger, W. Lotz, J. Nührenberg, and A. Schlüter, Proc. of the US-Japan Theory Workshop on 3D MHD Studies for Toroidal Devices, Oct. 19—21, 1981, ORNL-CONF-8110101, p. 51.
[7] K. C. Shaing and J. D. Callen, Report University of Wisconsin, UWFDM-416.
[8] H. E. Mynick, Phys. Fluids **25**, 325 (1982).
[9] W. Dommaschk, IPP-Report 0/38, 1978; Z. Naturforsch. **36a**, 251 (1981).
[10] R. G. Littlejohn, Phys. Fluids **24**, 1730 (1981).
[11] S. Gill, Proc. Camb. Phil. Soc. **47**, 96 (1951).
[12] G. G. G. Lister, D. E. Post, and R. Goldston, in 3rd Varenna Symposium on Plasma Heating in Toroidal Devices (Editrice Composotori, Bologna, Italy, 1976), p. 303.
[13] D. Pfirsch and A. Schlüter, Report MPI/PA 17/62, Max-Planck-Institut für Physik und Astrophysik, München 1962.
[14] A. A. Galeev and R. Z. Sagdeev, Sov. Phys. JETP **26**, 233 (1968).
[15] D. A. Anderson and H. P. Furth, Nucl. Fusion **12**, 207 (1972).
[16] T. Stringer, Nucl. Fusion **12**, 689 (1972).